ISIJ International, Vol. 34 (1994), No. 2, pp. 205–210

Role of Eta-carbide Precipitations in the Wear Resistance Improvements of Fe–12Cr–Mo–V–1.4C Tool Steel by Cryogenic Treatment

Fanju MENG, Kohsuke TAGASHIRA, Ryo AZUMA and Hideaki SOHMA[1)]

Muroran Institute of Technology, Department of Mechanical Engineering, Mizumoto, Muroran, Hokkaido, 050 Japan.
1) Muroran Techno-Center, Higashimachi, Muroran, Hokkaido, 050 Japan.

(Received on July 8, 1993; accepted in final form on November 19, 1993)

The wear resistance of an Fe–12.2wt%Cr–0.84wt%Mo–0.43wt%V–1.44wt%C alloy tool steel after cold treatment at 223 K (subzero treatment) and after cryogenic treatment at 93 K (ultra-subzero treatment) has been investigated. The wear resistance of steels after cryogenic treatment is superior to that after cold treatment. The effects of cryogenic treatment on the microstructure were also studied by means of X-ray diffraction and transmission electron microscopy methods. Unlike cold treatment, cryogenic treatment improves the preferential precipitation of fine η-carbides instead of ε-carbides. These fine carbide particles enhance the strength and toughness of the martensite matrix and then increase the wear resistance. The formation mechanism of fine η-carbide is discussed.

KEY WORDS: alloy tool steel; wear resistance; subzero treatment; cryogenic treatment; precipitation; η-carbide; retained austenite.

1. Introduction

Cold treatment (subzero treatment), as an indispensable part of heat treatment of alloy tool steels, offered significant increases in the wear resistance. It is widely accepted that a major factor contributing toward its success is the removal of retained austenite.[1)] Conventional cold treatment has been carried out at higher than 173 K. This temperature is believed to be sufficient to fully transform any retained austenite to martensite in the quenched microstructure. However, more recent evidence has shown that wear resistance is further enhanced by cryogenic treatment at ultra-low temperature (ultra-subzero treatment), such as liquid nitrogen temperature.[1-4)] Despite the numerous practical successes of cryogenic treatment and research projects undertaken worldwide, no conclusive metallurgical understanding of this treatment has been established.

A wide range of experimental techniques has been applied to investigate the atomic displacement of carbon and microstructural changes in martensite during tempering, including X-ray diffraction,[5-7)] electron microscopy and diffraction,[8-11)] Mössbauer spectroscopy,[12)] atom probe field ion micrscopy,[13)] electrical resistivity,[9)] dilatometric and calorimetric analysis.[14)] According to the present state of knowledge the structural evolution of martensite on tempering can be divided into the following sequence of processes: (a) the 0-th stage, the formation of carbon atom clusters, modulated structures and ordered structures, (b) the first stage, where the martensite decomposes into low carbon martensite containing 0.2 to 0.3 wt% C and ε-transition carbide particle, (c) the second stage, the decomposition of retained austenite into ferrite and cementite, (d) the third stage, conversion of the transition carbide into cementite and complete loss of the tetragonality of martensite.

Although a lot of works about tempering behavior have been done, a complete and satisfactory understanding of the mechanisms of the structural changes involved has not yet been obtained. The 0-th stage, *i.e.*, prior to carbide precipitation, and the first stage were of interest in the last decades. However, not so much attention has been paid to studying the effects of cryogenic treatment on the carbide precipitation in martensite during tempering.

The aims of the present study, therefore, are to investigate metallurgically the wear resistance and the microstructure of tempered alloy tool steels after quenching, after cold treatment at 223 K and after cryogenic treatment at 93 K.

2. Experimental Procedure

Alloy tool steel with composition (wt%), 1.44C, 0.3Si, 0.4Mn, 12.2Cr, 0.84Mo, 0.43V, 0.022P and 0.008S was used. Heat treatment was performed at a constant heating rate of 0.17 K/s up to 1 073 K in a vacuum furnace at 4×10^{-3} Pa, then up to austenitizing temperature of 1 293 K or 1 373 K with a nitrogen atmosphere at 20 Pa, followed by quenching to room temperature and aging at 333 K to avoid crack. The martensite start temperature (M_s) of this alloy is approximately 373 K. Cold treatment at 223 K and cryogenic treatment at 93 K were carried out. **Figure 1** shows a typical heat treatment

cycle of experiments.

The specimens for the wear resistance with a size $25 \times 50 \times 10$ mm were ground and polished mechanically after tempering at 453 K for 1.8 ks. A schematic diagram of a sample-on-wheel wear test machine is shown in **Fig. 2**. A friction wheel which has the same chemical composition as the specimens was quenched and tempered with a hardness HV780. No lubrication was used. The friction wheel rotated at a peripheral speed from 0.5 to 3.62 m/s, the sliding distance was from 200 to 600 m and the applied load was 21N. The wear rate, $W_s = Bb^3/8rPL$, was calculated, where B is thickness of the wheel, b is width of wear, r is the radius of the wheel, P is the applied load, and L is the sliding distance.

The volume fraction of retained austenite was determined by X-ray phase analysis at room temperature. Peaks {211} of martensite and peaks {311} of the retained austenite were employed.

The thin sheets of approximately 100 μm in thickness for the observation of transmission electron microscopy (TEM) were austenitized and quenched by the same condition as mentioned above. The pressure of nitrogen atmosphere at 20 Pa was controlled in order to avoid decarburization due to oxidation and/or evaporation during heat treatment. According to chemical analysis, the carbon content of the heat treated sheets has been confirmed to be unchanged. Tempering was carried out at 453 K for 600 s after cold treatment and cryogenic treatment. The ϕ 3 mm discs were punched and jet-polished to perforation using an electrolyte of 10% $HClO_4$ and 90% CH_3COOH at 283 K.

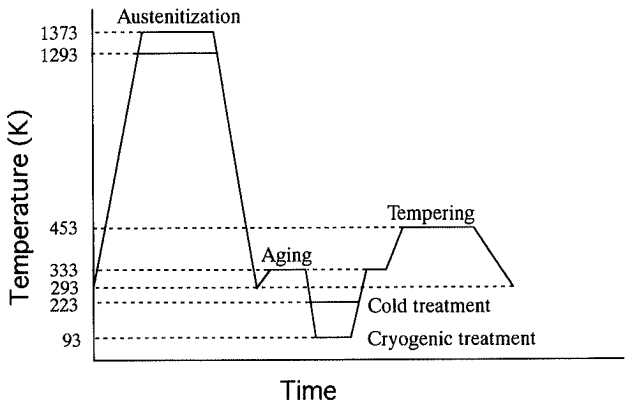

Fig. 1. Schematic representation of heat treatment.

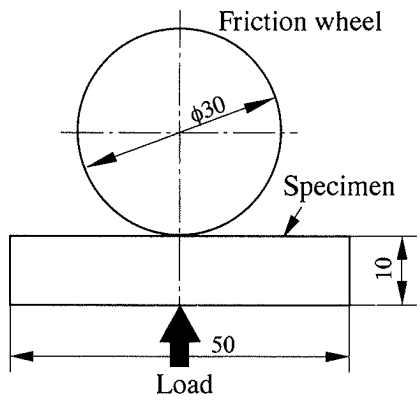

Fig. 2. Schematic diagram of a sample-on-wheel wear test machine.

3. Results

3.1. Wear Resistance

The variation of the wear rate with sliding speed is shown in **Fig. 3** for specimens austenitized at 1 293 K, quenched and ultra-subzero treated at 93 K. Finally tempering was carried out at 453 K for 1.8 ks. The wear rate of specimens after cryogenic treatment is smaller than that of as-quenched specimens (without any subzero treatment) for whole sliding speed. Furthermore, it decreases dramatically at high sliding speed. The cryogenic treatment results show 110 to 600% improvement. The wear rate shows a minimum at the sliding speed of 1.14 and 1.63 m/s for specimens without and with cryogenic treatment, respectively.

In **Fig. 4**, the variation of the wear rate with sliding distance is shown for specimens quenched, subzero treated at 223 K and ultra-subzero treated at 93 K. The wear rate of as-quenched specimens is larger than that of specimens after cold treatment and cryogenic treatment at sliding distance 200 m. At sliding distance 400 and 600 m, the specimens after cold treatment have al-

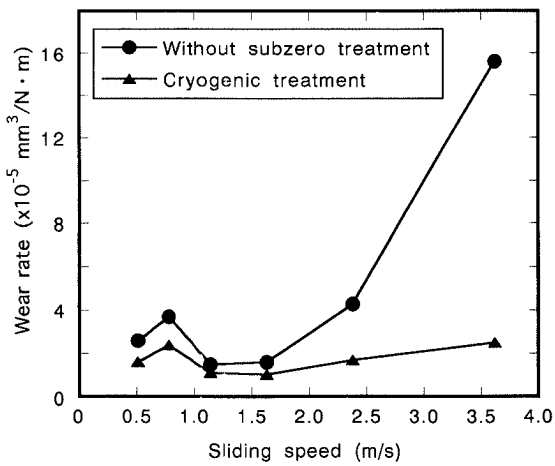

Fig. 3. Wear rate *vs.* sliding speed for specimens both with and without cryogenic treatment, austenitization at 1 293 K and tempering at 453 K for 1.8 ks. Sliding distance is 200 m.

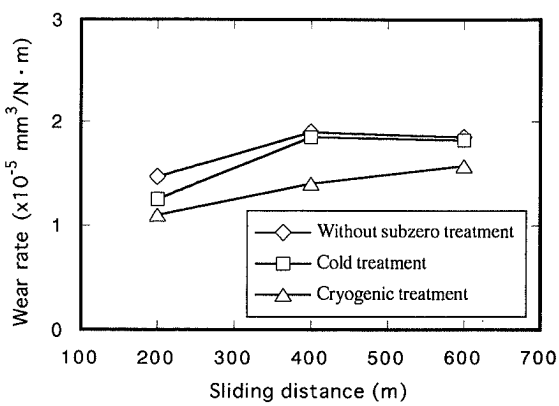

Fig. 4. Wear rate *vs.* sliding distance for specimens quenched, subzero treated at 223 K and ultra-subzero treated at 93 K, austenitization at 1 293 K and tempering at 453 K for 1.8 ks. Sliding speed is 1.14 m/s.

most the same wear rate as as-quenched specimens. However, the specimens after cryogenic treatment have a smaller wear rate than as-quenched specimens and specimens after cold treatment for any sliding distance.

3.2. X-Ray Diffraction Analysis

The volume fraction of retained austenite is plotted against the subzero treatment temperature in **Fig. 5** for specimens austenitized at 1 293 and 1 373 K. The volume fraction of retained austenite is 12% for as-quenched specimens after austenization at 1 293 K, and approximately 6% for specimens after cold and cryogenic treatment. However, it decreases with treating temperature going down for specimens austenitized at 1 373 K.

Cold treatment reduces the volume fraction of retained austenite drastically. Nevertheless, cryogenic treatment reduces it slightly relative to cold treatment.

3.3. Structure Observation of TEM

3.3.1. As-quenched and Tempered Structure

The microstructure of as-quenched specimens consists of mainly fine twinned martensite and retained austenite, the spacing between twins being a few tens nm.

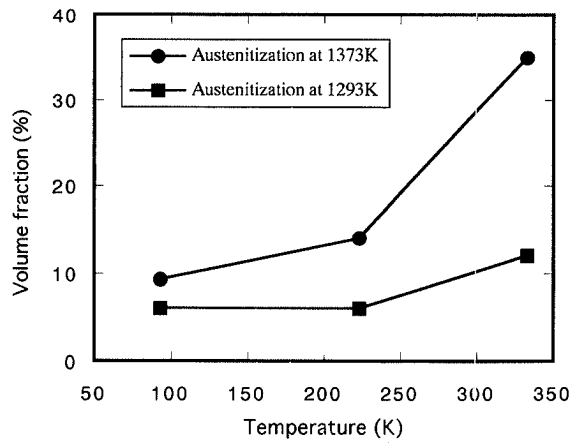

Fig. 5. Volume fraction of retained austenite *vs.* subzero treatment temperature.

The bright-field image of **Fig. 6** shows the microstructure of specimens quenched and tempered at 453 K for 600 s. The structure is mainly constructed with martensite and retained austenite. In the martensitic regions, many plates are internally twinned and some of the twins are extremely fine, the spacing between twins being a few tens nm. On close examination, the twinned martensite shows coarse striated structure, which has been interpreted as the modulated structure produced by the spinodal decomposition, *i.e.*, two variants of the carbon-rich regions. But there is a great difference from the results of Taylor and others.[9,11] Only one set of fine parallel line contrasts was seen in the bright-field image. The fine striations were spaced about 1 nm apart on average.

3.3.2. Microstructure after Cold Treatment

Figure 7(a) shows the bright-field image of specimens subzero treated at 223 K and then tempered. Coarse tweedlike structure corresponding to two orientation variants was present. This fine scale modulated structure has a wavelength of about 5 nm. However, carbide

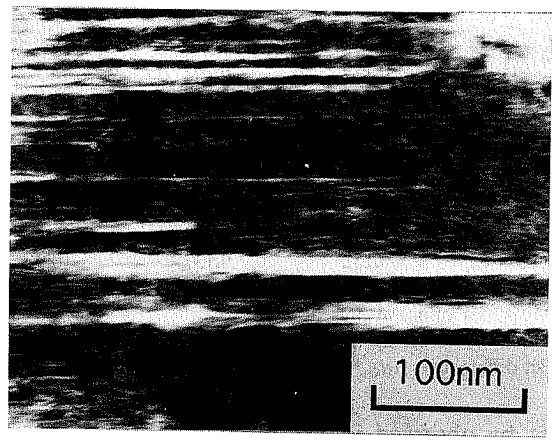

Fig. 6. Transmission electron micrograph of a specimen tempered at 453 K for 600 s without subzero treatment, showing a striated structure.

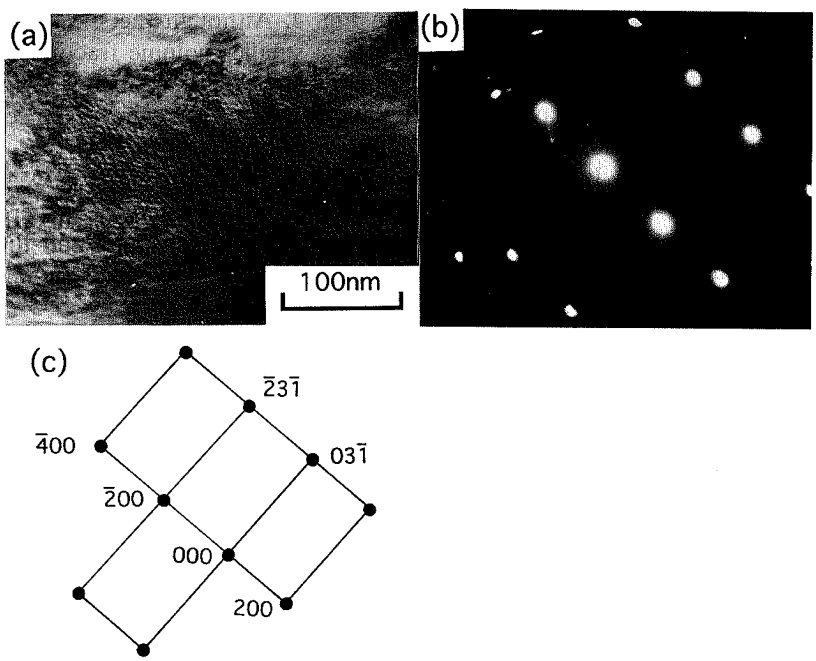

Fig. 7.
(a) Bright-field electron micrograph of a specimen subzero treated at 223 K and tempered, showing a tweedlike structure.
(b) Electron diffraction pattern taken from the tweedlike structure.
(c) Indexed pattern of (b).
Beam//$[013]_{\alpha'}$.

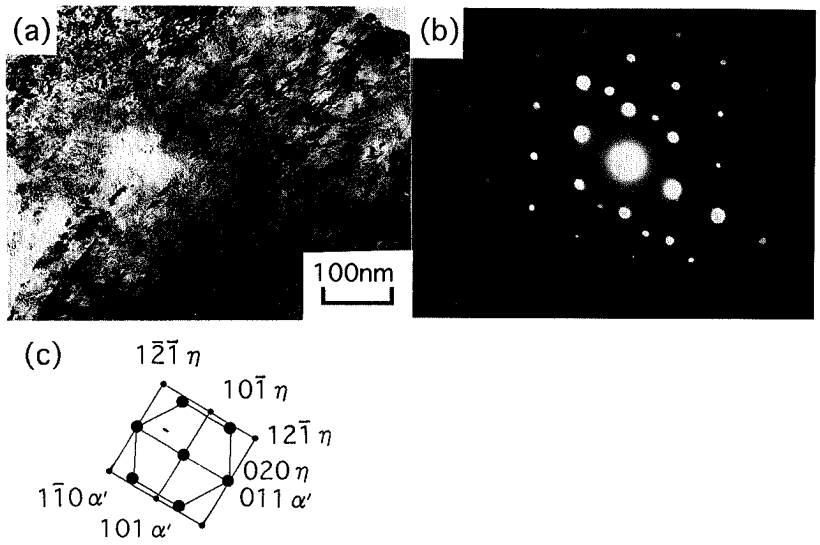

Fig. 8.
(a) Transmission electron micrograph of carbide precipitation in a specimen ultra-subzero treated at 93 K and tempered.
(b) Electron diffraction pattern, showing two zonal patterns from martensite matrix and η-carbide.
(c) Indexed pattern of (b).
Beam//$[11\bar{1}]_{\alpha'}$//$[101]_{\eta}$.

Table 1. Comparison of interplanar spacings for η- and ε-carbide.

hkl	d_{hkl}*1 (nm)	d_{hkl}*2 (nm)	Pct difference*3
	η-carbide indexing[8]		
(101)	0.229	0.242	5.3
(020)	0.211	0.215	1.8
(121)	0.154	0.161	4.3
	ε-carbide indexing[15]		
(002)	0.223	0.216	−3.2
(101)	0.211	0.208	−1.4
(110)	0.152	0.137	−10.9

*1 Measured values at present work.
*2 Published values by Refs. 8) and 15).
*3 Pct difference $=[(d_{hkl}{}^{*2}-d_{hkl}{}^{*1})/d_{hkl}{}^{*2}]\times 100$.

cannot be observed in the modulated microstructure. **Figures 7(b)** and **7(c)** are the selected area diffraction pattern and the indexed pattern respectively, which consists of a [013] martensite zone. Inspection of diffraction pattern revealed streaking due to spinodal decomposition during the 0-th stage of tempering.

3.3.3. Microstructure after Cryogenic Treatment

The microstructure of the martensite after cryogenic treatment and tempering was remarkably changed, shown in **Fig. 8(a)**. In most of the areas appeared fine carbide particles developed in the boundary of twins. In different areas, fine carbide particles appeared at the points which have a considerable diffusing density. Some rodlike carbide particles parallel to each other appeared and varied in size from 5 to 10 nm in cross-section and from 20 to 40 nm in length.

Figures 8(b) and **8(c)** are the selected area diffraction pattern and the indexed pattern, respectively. The diffraction pattern consists of a $[11\bar{1}]$ martensite zone and a [101] η-carbide zone. It was seen that the (011) martensite plane is parallel to the (010) η-carbide plane, the $[11\bar{1}]$ martensite direction is parallel to the [101] η-carbide direction. From this pattern, it could be confirmed that the orientation relationship between martensite (α') and η-carbide is the Hirotsu and Nagakura relationship,[8] as indicated below:

$$(011)_{\alpha'}//(010)_{\eta};\ [11\bar{1}]_{\alpha'}//[101]_{\eta}.$$

Jack[15] identified transition carbide which forms during tempering between 350 and 430 K as hexagonal ε-carbide. **Table 1** compares the difference associated with the indexing of the carbide diffraction pattern according to published values of d_{hkl} for η- and ε-carbide. Although there is a close similarity between the structure of η- and ε-carbide, it is clear that the precipitated phase is η-carbide rather than ε-carbide.

4. Discussion

4.1. Relationship between Wear Resistance and Retained Austenite

From Fig. 5, the specimens austenitized at 1 293 K, subzero treated at 223 K and ultra-subzero treated at 93 K have almost the same volume fraction of the retained austenite. However, the specimens after cryogenic treatment show wear resistance improvement considerably, as shown in Fig. 4. Although the specimens after cold treatment have a smaller volume fraction of the retained austenite than that of the as-quenched ones, both have almost the same wear rate at sliding distances 400 and 600 m.

It is accepted that a major factor contributing to wear resistance improvement through subzero or ultra-subzero treatment is the removal of retained austenite and the formation of homogeneous martensitic structure although the hardness is hardly changed.[16,17]

According to the scanning electron microscopy observation of the worn surface of hardened carbon tool steel tempered at temperature lower than 573 K by Hu *et al.*,[18] the predominant wear mechanisms were ploughing fatigue, fracture, and delamination. In this case, the wear rate may be controlled by crack nucleation and propagation beneath the surface, which is related to the strength and toughness of the materials. Retained austenite may prevent crack propagation either by changing the growth direction of an advancing crack or by great energy absorption. It is suggested that cryogenic

treatment makes a contribution to wear resistance due to fine η-carbide precipitation rather than the removal of retained austenite.

4.2. Mechanism of η-carbide Precipitation

A model of the bct-orthorhombic system transformation is proposed. It is known that the lattice deformation of martensite results from cryogenic treatment.[5,19] **Figures 9(a)** and **9(b)** represent the relationship between (010) η-carbide plane and (110) martensite plane. This existance of the lattice correspondence between two phases implies that (010) η-carbide plane is derived from (110) martensite plane, and [100], [010] and [001] η-carbide directions are derived from $[\bar{1}10]$, [110] and $[00\bar{1}]$ martensite directions respectively. In the η-carbide structure, carbon atoms are in the octahedral interstices and iron or substitutional atoms take a hcp arrangement. The distance between neighbor iron atoms or substitutional atoms in η-carbide and martensite is $\overline{AB}(\eta) > \overline{AB}(\alpha')$, $\overline{BC}(\eta) < \overline{BC}(\alpha')$.

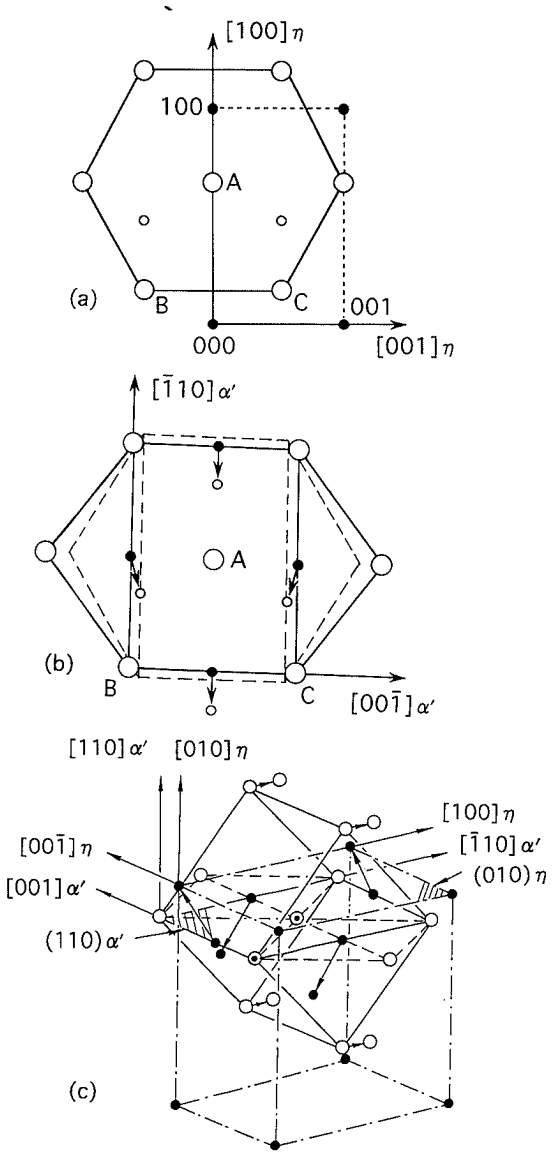

Fig. 9. Atom arrangement on (010) η-carbide plane including a projection along $[010]_\eta$[8] (a) and (110) martensite plane (b). Distortion of lattice and shift of carbon atom converts the bct lattice into the orthorhombic lattice. These transform the solid rectangle into the dashed rectangle. (a): (●), carbon atom at 0; (○), carbon atom at $1/2[010]_\eta$; (○) iron or substitutional atom at $1/4[010]_\eta$. (b): (●), carbon atom before transformation from martensite to η-carbide, (○), carbon atom after transformation, (○), iron or substitutional atom. (c) The bct-orthorhombic system transformation.

The lattice deformation is supposed to convert the parent bct lattice into an orthorhombic η-carbide lattice through the readjustment of iron or substitutional atoms due to contraction along $[\bar{1}10]$ and [110] martensite direction and expansion along [001] martensite direction. Correspondingly, a sligh shift of carbon atoms is required on (110) martensite planes in order to achieve carbon atom stacking of η-carbide. This can be present as follows in bct lattice, carbon atoms at (1/2, 1/2, 0) and (1/2, 1/2, 1) positions in (110) martensite plane shift $a/12[\bar{1}\bar{5}0]$, which may be explained $a/6[1\bar{1}0] + a/4[\bar{1}\bar{1}0]$, and ones at (0, 1, 1/2) and (1, 0, 1/2) positions shift $a/12[510]$, *i.e.*, $a/6[1\bar{1}0] + a/4[110]$, where a means the lattice parameter of martensite. Furthermore, before contraction and expansion, a $a/6[\bar{1}10]$ shuffling of iron or substitutional atoms on alternate (110) martensite plane is necessary to meet the needs of stocking described by η-carbide structure. Alternatively, iron or substitutional atoms and carbon atoms in the other (110) martensite planes also change correspondingly as indicated above. **Figure 9(c)** shows the bct-orthorhombic system transformation. The plain circle indicate iron or substitutional atoms, the double circles indicate iron or substitutional atoms which belong to two unit cells and the solid circles indicate carbon atoms. The shuffling direction of atoms is shown by an arrow. It is suggested by TEM observation and crystallographic analysis of carbide that carbide nucleates heterogeneously along the carbon-rich bands which develop during the spinodal decomposition of martensite.[9]

It is well known that precipitation of fine η-carbide enhances strength and toughness of martensite matrix, and further increases wear resistance.[2,20]

5. Conclusions

(1) Cryogenic treatment increases wear resistance dramatically, especially at high sliding speed. The specimens after cryogenic treatment show a minimum of wear rate.

(2) Unlike cold treatment, cryogenic treatment promotes preferential precipitation of fine η-carbides.

(3) The formation mechanism of η-carbide is supposed to be as follows: iron or substitutional atoms expand and contract, and carbon atoms shift slightly due to lattice deformation as a result of cryogenic treatment.

(4) The mechanism that cryogenic treatment contributes to wear resistance is through the precipitation of fine η-carbide, which enhances strength and toughness of martensite matrix, rather than the removal of the retained austenite.

Acknowledgments

The authors wish to thank technician Mr. H.

Yamamori and graduate student Mr. T. Nakamura of Muroran Institute of Technology for their helpful co-operation in the experiment. Part of the investigation was carried out with the financial support of Senju Metal Industry Co., Ltd.

REFERENCES

1) R. B. Reasbeck: *Metallurgia*, **56** (1989), 178.
2) T. P. Sweeney: *Heat Treating*, Feb., (1986), 28.
3) L. Yu and X. Feng: *Metal Heat Treatment*, **1** (1991), 24.
4) M. Yamanaka, E. Tsunazawa and K. Yamanaka: *Heat Treatment*, **31** (1991), 331.
5) H. Hayakawa, M. Tanigami and M. Oka: *Metall. Trans.*, **16A** (1985), 1745.
6) L. Cheng, N. M. van der Pers, A. Bottger, Th. H. de Keijser and E. J. Mittemeijer: *Metall. Trans.*, **22A** (1991), 1957.
7) L. Cheng, A. Bottger and E. J. Mittemeijer: *Metall. Trans.*, **23A** (1992), 1129.
8) Y. Hirotsu and S. Nagakura: *Acta Metall.*, **20** (1972), 645.
9) K. A. Taylor, G. B. Olson, M. Cohen and J. B. Vander Sande: *Metall. Trans.*, **20A** (1989), 2749.
10) O. N. C. Uwakweh, J.-M. R. Genin and J.-F. Silvain: *Metall. Trans.*, **22A** (1991), 797.
11) Y. Ohmori and I. Tamura: *Metall. Trans.*, **23A** (1992), 2147.
12) O. N. C. Uwakweh, J. Ph. Bauer and J.-M. R. Génin: *Metall. Trans.*, **21A** (1990), 589.
13) M. K. Miller, P. A. Beaven, S. S. Brenner and G. D. W. Smith: *Metall. Trans.*, **14A** (1983), 1021.
14) L. Cheng and E. J. Mittemeijer: *Metall. Trans.*, **21A** (1990), 13.
15) K. H. Jack: *J. Iron Steel Inst.*, **169** (1951), 26.
16) T. Okawa, K. Ishimatsu and Y. Nagata: *Heat Treatment*, **17** (1987), 86.
17) S. Owaku: *Heat Treatment*, **21** (1981), 44.
18) J. Hu, Z. Li, Y. Wang and X. Bu: *Mater. Sci. Technol.*, **8** (1992), 796.
19) F. E. Fujita: *Metall. Trans.*, **8A** (1977), 1727.
20) E. A. Carlson: ASM Handbook, Vol. 4, (1991), 203.